physica status solidi b
www.pss-b.com

Electrical and Optical Properties of hBN Capped $MoTe_2$ Monolayers Fabricated by Gold-Mediated Exfoliation

*Taku Yoshimura, Hiroshi Shigeno, Rikuto Yamamura, Kenji Watanabe, Takashi Taniguchi, and Yusuke Hoshi**

This study focuses on the electrical and optical properties of monolayer $MoTe_2$ (1L-$MoTe_2$) flakes fabricated via gold-mediated exfoliation, and it is demonstrated that this technique applies to the development of 1L-$MoTe_2$ channel field-effect transistors (FETs). The average area of the gold-exfoliated flakes is larger than that of conventional tape exfoliation. While the samples without an hBN cap layer are easily oxidized by atmospheric exposure for 1 day, increasing the number of nonradiative recombination centers, the surface oxidation of 1L-$MoTe_2$ can be suppressed by the deposition of the hBN cap layer. The transfer characteristics of the 1L-$MoTe_2$ channel FETs show clear ambipolar behavior and excellent switching properties, with an on/off ratio of 10^5. It is shown that graphite/1L-$MoTe_2$ junctions form a Schottky barrier with an energy of 280 meV, consistent with the theoretical value. By lowering the vacuum level, the gate voltage at the conductivity minimum point shifts to a negative value and the subthreshold swing decreases, implying a reduction in the interfacial trapped charge density due to the physisorption of O_2/H_2O molecules. These results demonstrate that the electrical properties of gold-exfoliated 1L-$MoTe_2$ strongly depend on the environmental conditions.

1. Introduction

Transition metal dichalcogenides (TMDCs) have attracted considerable research interest owing to their distinct band structures and unique properties in ideal and atomically thin 2D systems. In particular, TMDCs with a monolayer (1L) thickness are recognized as advanced materials for use in nano- and microelectronic devices with various functionalities, taking advantage of features such as an ultrahigh surface-to-volume ratio and piezoelectricity resulting from the spatial inversion symmetry breaking of crystal structures.[1–3] Recently, 1L-TMDCs have been employed in developing gas and chemical sensors owing to their exceptional sensitivity to selected gases and environmental conditions.[4–6] Among the different sensing technologies, semiconductor-based field-effect transistor (FET) sensors offer high potential for realizing mass production owing to their low cost, miniaturization, and high compatibility with conventional Si-based device fabrication processes. The FET-type sensors operate by detecting the change in the resistance of the 1L-TMDCs owing to the charge transfer resulting from the adsorption of gas molecules on the channel surface.[6–9] Therefore, understanding the effect of environmental conditions on the electrical properties of 1L-TMDC channel FETs is crucial for improving sensor performance.

The semiconducting molybdenum ditelluride monolayer (1L-$MoTe_2$) exhibits outstanding ambipolar carrier transport compared to other TMDC-based materials and an optical bandgap of 1.1 eV, close to that of Si.[10–14] In addition, $MoTe_2$ FET sensors exhibit high sensitivity and excellent reversibility at room temperature for various gases such as O_2, NO_2, and NH_3 detection.[7,15,16] 1L-$MoTe_2$ flakes are usually prepared by a mechanical tape exfoliation technique because high-quality crystals can be obtained. However, the resultant crystal size is small, and the production yield is poor compared to that of other TMDCs. Chemical vapor deposition (CVD) can be used to grow large-area monolayer and multilayer $MoTe_2$, but the resultant crystal quality is inferior to that produced by mechanical tape exfoliation.[17,18] In addition, the growth processes for producing semiconducting $MoTe_2$ must be sophisticated owing to the small difference in the formation energy between the semiconducting (2H) and metallic (1T′) phases.[19] Recently, gold-mediated exfoliation, a technique for peeling off the top monolayer of bulk crystals using the strong adhesion of gold to TMDCs, has been reported to enable the formation of large-area TMDC monolayers.[20–22] The monolayer flakes are macroscopic in

T. Yoshimura, H. Shigeno, R. Yamamura, Y. Hoshi
Advanced Research Laboratories
Tokyo City University
1-28-1 Tamazutsumi, Setagaya-ku, Tokyo 158-8557, Japan
E-mail: yhoshi@tcu.ac.jp

K. Watanabe
Research Center for Electronic and Optical Materials
National Institute for Materials Science
Tsukuba 305-0044, Japan

T. Taniguchi
Research Center for Materials Nanoarchitectonics
National Institute for Materials Science
Tsukuba 305-0044, Japan

The ORCID identification number(s) for the author(s) of this article can be found under https://doi.org/10.1002/pssb.202400374.

DOI: 10.1002/pssb.202400374

centimeter size, and the crystal quality of the 1L-TMDCs can be degraded during the chemical wet etching of gold films. In addition, 1L-$MoTe_2$ is easily oxidized upon exposure to air for several days owing to poor structural stability, leading to an increase in nonradiative recombination centers.[23,24] However, reports on device applications of 1L-$MoTe_2$ fabricated by gold-mediated exfoliation remain limited. In this study, we focus on the electrical and optical properties of 1L-$MoTe_2$ flakes prepared by gold-mediated exfoliation and demonstrated this technique applies to the development of 1L-$MoTe_2$ devices. Our device structures include an hBN cap layer and graphite source/drain electrodes on the 1L-$MoTe_2$ channels. hBN was stacked to avoid surface oxidation of the 1L-$MoTe_2$ flakes under atmospheric conditions and suppress crystal quality degradation due to the heating effects during device operation.[25–27] Graphite was chosen as the source/drain electrode since it is a layered metallic material that can be easily integrated into a van der Waals heterostructure and exhibits the work function featuring near-midgap energy in $MoTe_2$. The 1L-$MoTe_2$ channel FETs exhibit clear ambipolar behavior and switching properties, with an on/off ratio of ≈105. Furthermore, the vacuum level reduction strongly affects the electrical properties of 1L-$MoTe_2$ channel FETs due to the desorption of some molecules, which causes the charge transfer of electrons.

2. Results and Discussion

Figure 1a shows an optical microscopy image of the $MoTe_2$ sample prepared by gold-mediated exfoliation. The $MoTe_2$ flakes have some different contrast regions owing to different thicknesses in each region. Figure 1b represents a photoluminescence (PL) intensity map around photon energies of 1.05–1.17 eV in the area surrounded by the red dashed line in Figure 1a. The PL intensity is uniform over the area surrounded by the white dashed line, indicating the uniformity of the crystal quality in $MoTe_2$. As previously reported, the PL intensity strongly depends on the layer number owing to the band structure modulation; thus, the area with a large PL intensity corresponds to the thinner $MoTe_2$.[14] We measured the PL spectrum at room temperature to identify the number of layers in the $MoTe_2$ region with high PL intensity. Figure 1c shows a PL spectrum at the P1 position in Figure 1b. The spectrum has an intense peak at 1.09 eV owing to the radiative recombination of a neutral exciton, resulting in a monolayer of the $MoTe_2$ flake. Moreover, the spectrum also has a low-energy shoulder, which is tentatively attributed to the PL signals from the exciton–phonon interactions.[28,29] Figure 1d shows a representative Raman spectrum for the as-prepared 1L-$MoTe_2$ flakes. It is characterized by two prominent peaks based on the A_{1g} and E_{2g} vibration modes at 165 and 230 cm^{-1} and by the absence of a $B^1{}_{2g}$ mode at ≈290 cm^{-1}, which are typical signatures of 1L-$MoTe_2$.[14,30,31] Figure 1e shows histograms of the areas of the $MoTe_2$ flakes prepared by gold-mediated exfoliation and standard tape exfoliation techniques. The average area of the gold-exfoliated 1L-$MoTe_2$ flakes is 30 times larger than that of the tape exfoliation. The gold-mediated exfoliation technique enabled the formation of large-area 1L-$MoTe_2$ flakes with uniform crystal quality, demonstrating its usefulness for applications in 1L-$MoTe_2$ channel devices. The monolayer areas of $MoTe_2$ appear to be

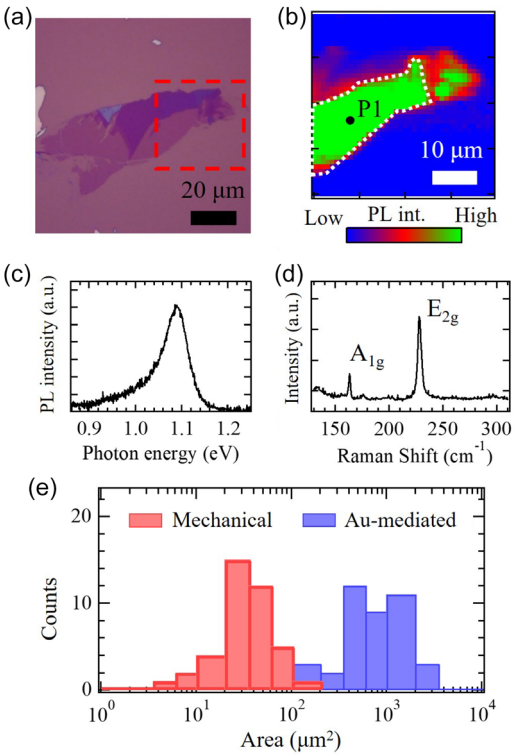

Figure 1. a) Optical microscope image of the gold-exfoliated $MoTe_2$ flake. b) PL intensity map in the area surrounded by red dashed line in (a). c) PL spectrum at the P1 position in (b). d) Raman spectrum of the 1L-$MoTe_2$ fabricated by Au-mediated exfoliation. e) Histogram of flake areas for conventional mechanical-exfoliated and gold-exfoliated 1L-$MoTe_2$.

smaller than those of the other TMDCs prepared by Au-mediated exfoliation, possibly owing to the differences in the crystal quality and size of the initial bulk crystal before gold deposition.

We measured the PL spectra of samples prepared by gold-mediated exfoliation to investigate the effect of atmospheric exposure under typical laboratory room light illumination on the crystal quality degradation of 1L-$MoTe_2$. **Figure 2**a shows the PL spectra of 1L-$MoTe_2$ with and without the hBN cap layer. The black traces correspond to the as-prepared samples while the red traces correspond to the samples exposed to air for 2 days. The PL intensity drastically reduces after atmospheric exposure for the sample without the hBN cap layer but not for the sample with the hBN cap layer. Figure 2b shows the PL intensities normalized to the intensity I_0 obtained from the as-prepared sample, plotted as a function of the atmospheric exposure time for samples with and without the hBN cap layer. For the sample without the hBN cap layer, the normalized PL intensities are reduced to less than 0.5 after 1 day. Note that the PL spectral shape, except for the PL intensity, is not changed even after the exposure time of 7 days (see Figure S2, Supporting Information). This indicates that the surface oxidation of the 1L-$MoTe_2$ enhances the nonradiative recombination rates of neutral excitons, rather than through the formation of defect-bound excitons that emit the photons at a lower energy than that of the neutral exciton. In contrast, the PL intensity of the samples with the hBN cap layer is almost constant, with no reduction in the PL intensity by atmospheric

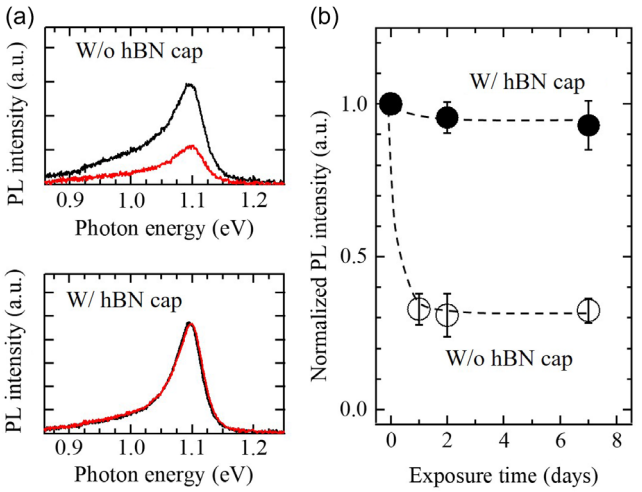

Figure 2. a) PL spectra for gold-exfoliated 1L-$MoTe_2$ with and without hBN cap layer. Black and red traces correspond to the as-prepared samples and the samples exposed to air for 2 days, respectively. b) Normalized PL intensity plotted as a function of exposure time in air. Filled and opened symbols represent the samples with and without hBN cap layer, respectively.

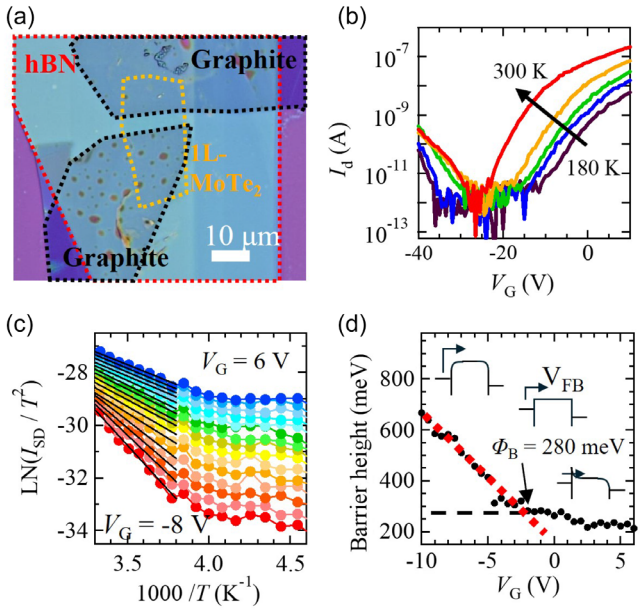

Figure 3. a) Optical microscope image of the 1L-$MoTe_2$ channel FET with graphite S/D electrodes. b) Temperature dependence of transfer characteristics in 1L-$MoTe_2$ channel FET with graphite contacts. c) ln(I_{SD}/T^2) is plotted against 1000/T at different back gate voltages. The solid lines represent a guide. d) Electron injection barrier height $q\Phi_B$ versus V_G for the FET, and extraction of Schottky barrier height (black dashed line). The inset shows the band configurations of the Schottky junction around the 1L-$MoTe_2$/graphite interfaces when the V_G is lower and higher than the flat band voltage V_{FB}.

exposure even after 30 days. These results indicate that the hBN cap layer effectively suppressed crystal quality degradation based on the surface oxidation of 1L-$MoTe_2$ prepared by gold-mediated exfoliation.

Electrical properties were measured to verify that the gold-mediated exfoliation technique is effective for developing large-area 1L-$MoTe_2$ channel devices with graphite source-drain contacts. **Figure 3**a shows an optical microscope image of a 1L-$MoTe_2$ channel FET. Figure 3b shows the I_{SD}–V_G characteristics as a function of temperature with V_G ranging from −40 to 10 V. The source-drain current increases when high positive and negative back-gate voltages are applied, indicating ambipolar transport behavior. In addition, excellent switching properties with a large on/off ratio of ≈105 were observed in the n-type operating regime at room temperature.

The Schottky barrier height was determined from the temperature-dependent transport characteristics using the following equation

$$I_{SD} = A^* T^2 \exp\left(-q\Phi_B/k_B T\right)\left\{1 - \exp\left(-qV_{SD}/k_B T\right)\right\} \quad (1)$$

where A^* is Richardson's constant, q is the elementary charge, k_B is Boltzmann's constant, T is the temperature, V_{SD} is the source-drain voltage of 0.5 V, and Φ_B is the potential barrier height measured from the Fermi level.[13,32] Notably, $\exp(-qV_{SD}/k_B T)$ is much smaller than unity under the experimental conditions. Therefore, the electron injection barrier energy $q\Phi_B$ can be estimated from the slope of the ln(I_{SD}/T^2) in the positive gate voltage region plotted as a function of 1000/T in Figure 3c according to Equation (1). Figure 3d shows the barrier height plotted as a function of back-gate voltage. The electron injection is divided into two schemes; at their boundary, the band configuration becomes a flat band condition. At a gate voltage smaller than the flat band voltage (V_{FB}), an electron injection barrier is formed at the graphite/1L-$MoTe_2$ interfaces owing to the band bending of 1L-$MoTe_2$ by applying the back-gate voltage; thus, the electron injection by the thermionic emission scheme dominates the current. A back-gate voltage larger than V_{FB} lowers the 1L-$MoTe_2$ band, and electrons accumulate in the 1L-$MoTe_2$ channel. Under a sufficiently high back-gate bias, the Schottky barrier becomes sufficiently thin to allow thermally assisted tunneling of electrons. As the barrier height does not change under a large back-gate bias condition, the tunneling component begins to dominate the current. Considering these band configurations, the injection barrier energy $q\Phi_B$ at $V_G = V_{FB}$ corresponds to the Schottky barrier height; the $q\Phi_B$ value can be estimated to be ≈0.28 eV. The Schottky barrier height is consistent with the theoretical values calculated from the work functions of graphite (≈4.7 eV) and n-type $MoTe_2$ (≈4.49 eV).[11,33]

We measured the transfer characteristics of hBN/1L-$MoTe_2$ channel FETs at room temperature at different vacuum levels to investigate the effect of environmental conditions on the electrical properties of 1L-$MoTe_2$. **Figure 4**a shows the dependence of the I_{SD}–V_G properties of a 1L-$MoTe_2$ channel FET on the vacuum level. The transfer curves of the device exhibit symmetrical ambipolar characteristics. The carrier mobilities are estimated to be 0.8–1.1 $cm^2\,Vs^{-1}$ for electrons and 0.6–1.0 $cm^2\,Vs^{-1}$ for holes independent of the vacuum level, which are comparable to the previously reported values in the few-layer $MoTe_2$ channel FETs.[10,12,34,35] Figure 4b shows the back-gate voltage at the conductivity minimum point (V_{CMP}) plotted as a function of vacuum level. The V_{CMP} gradually shifts to negative values due to electron

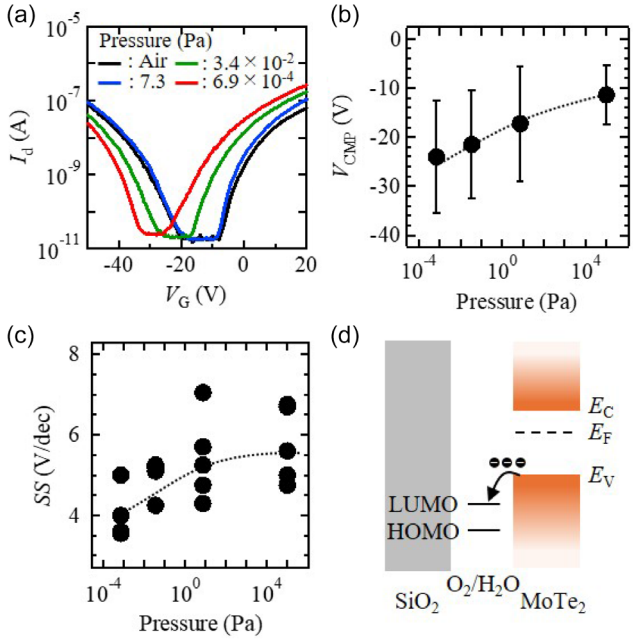

Figure 4. a) Transfer characteristics at different vacuum levels for the 1L-$MoTe_2$ channel FET. b) Back gate voltage at conductivity minimum point V_{CMP} and c) subthreshold swing in p-type regime plotted as a function of the vacuum levels. d) Schematic diagram illustrating charge transfer between 1L-$MoTe_2$ and O_2/H_2O molecules.

doping as the vacuum level decreases. The change in sheet electron density by the reduced pressure can be calculated as $\Delta n_{2d} = \Delta V_{CMP} C_g/q$ where ΔV_{CMP} is the back-gate voltage shift at the conductivity minimum point by the reduced pressure from atmospheric pressure to 6.9×10^{-4} Pa, and C_g is the gate oxide capacitance per unit area. The increase in the sheet electron density by the reduced pressure is found to be $1.3 \times 10^{12}\,cm^{-2}$. To confirm the pressure-dependent electron density modulation in the 1L-$MoTe_2$, we investigated the dependence of pressure on a PL spectrum (see Figure S3, Supporting Information). Radiative recombination of neutral excitons dominates under atmospheric conditions, indicating that the 1L-$MoTe_2$ channel is nearly intrinsic. As the pressure is reduced, the exciton PL intensity decreases monotonically due to the increased trion nonradiative recombination rates.[36] This result supports that the reduced pressure increases the electron density in the 1L-$MoTe_2$. It has been reported that when O_2/H_2O molecules are adsorbed on the 1L-$MoTe_2$ channel, electrons are transferred from the valence band of 1L-$MoTe_2$ to the energy level of the lowest unoccupied molecular orbits (LUMO) of the O_2/H_2O molecules, that is a hole doping to 1L-$MoTe_2$ (Figure 4d).[37–39] Therefore, the reduced pressure is believed to cause the desorption of the O_2/H_2O molecules physically adsorbed on 1L-$MoTe_2$ and to increase the electron density. In this device structure, the hBN cap layer is deposited on the 1L-$MoTe_2$ channel. As the hBN/1L-$MoTe_2$ interface is atomically flat, the molecules exist at the interface between 1L-$MoTe_2$ and SiO_2 rather than at the hBN/1L-$MoTe_2$ interface and are desorbed by lowering the vacuum level.[40,41]

Assuming that all the O_2/H_2O molecules physically adsorbed on 1L-$MoTe_2$ are desorbed by reducing the vacuum level, we can quantitatively estimate the molecular density from the variation of the trapped charge density between the atmospheric conditions and the reduced pressure. We evaluated the trapped charge density using a method similar to that in ref. [10]. In 2D systems, the density of the interfacial trapped charge is obtained via the subthreshold swing (SS) as follows

$$SS = \left(k_B T/q\right)\ln(10)\left(1 + C_{it}/C_g\right) \quad (2)$$

where k_B is the Boltzmann constant, T is the temperature, and C_{it} is the interfacial charge capacitance. The trapped charge density is given by $D_{it} = C_{it}/q$. Since the physisorbed O_2/H_2O molecules lead to the electron transfer from the valence band of the 1L-$MoTe_2$, we focus on the SS variation in the p-type regime by reducing the vacuum level (Figure 4c). Under atmospheric conditions, the SS is $5.5\,V\,dec^{-1}$, corresponding to a trapped charge density of $6.8 \times 10^{12}\,cm^{-2}$, while it is reduced to $4.2\,V\,dec^{-1}$, corresponding to $5.2 \times 10^{12}\,cm^{-2}$, by lowering the pressure to 6.9×10^{-4} Pa. Thus, the density of the molecules physically adsorbed on the 1L-$MoTe_2$ is estimated to be $1.6 \times 10^{12}\,cm^{-2}$, which is consistent with the aforementioned sheet electron density variation Δn_{2d} calculated from the V_{CMP} shift by lowering the vacuum level. These results demonstrate that the phenomenon of pressure-dependent changes in the electrical properties of the 1L-$MoTe_2$ channel FETs is responsible for the electron transfer based on the adsorption and desorption of O_2/H_2O molecules. In fact, we have confirmed that the pressure-dependent transport behavior in the 1L-$MoTe_2$ channels does not occur in the N_2 environment. On the other hand, in the n-type regime, SS seems to increase under reduced pressure. Since physisorbed molecules are removed under reduced pressure, the van der Waals gap between 1L-$MoTe_2$ and SiO_2 becomes small. Thus, electrons in the conduction band of 1L-$MoTe_2$ may be trapped by the surface states on SiO_2.

There is concern that the presence of physisorbed O_2/H_2O molecules at the 1L-$MoTe_2$/SiO_2 interface promotes oxidation of the 1L-$MoTe_2$. Kotsakidis et al. analyzed the surface oxidation of CVD-grown WS_2 and found that oxidation is observed upon excitation of an electronic transition such as light irradiation for the WS_2 areas containing more defects.[42] In 1L-$MoTe_2$, the typical laboratory room light easily excites carriers due to the small optical bandgap of 1.09 eV, and thus, oxidation should proceed due to the presence of O_2/H_2O molecules physisorbed at the 1L-$MoTe_2$/SiO_2 interface. However, the PL signals obtained from the hBN/1L-$MoTe_2$ structures are stable even after long-term exposure to air under laboratory room light illumination as shown in Figure 2c, indicating that the surface oxidation of the 1L-$MoTe_2$ is sufficiently suppressed. This phenomenon is explained as follows. The surface oxidation of the 1L-$MoTe_2$ proceeds with the formation of crystal defects in the 1L-$MoTe_2$, rather than by chemical reactions involving redox oxidation with O_2/H_2O molecules. In our case, the 1L-$MoTe_2$ channels are covered by hBN multilayers, which effectively suppress the formation of crystal defects such as Te vacancies in the 1L-$MoTe_2$.[25] Therefore, it is believed that the oxidation does not proceed by the presence of O_2/H_2O molecules physisorbed at the interface between the 1L-$MoTe_2$ and SiO_2 although the charge transfer occurs.

3. Conclusion

We investigated the electrical and optical properties of 1L-$MoTe_2$ flakes prepared by the gold-mediated exfoliation. The average area of the fabricated 1L-$MoTe_2$ was ≈30 times larger than that obtained by conventional tape exfoliation. In addition, surface oxidation of 1L-$MoTe_2$ after exposure to air for 1 day occurred for the samples without the hBN cap layer, leading to an increase in nonradiative recombination centers. In contrast, oxidation was sufficiently suppressed for the samples with hBN. The transfer characteristics of the 1L-$MoTe_2$ channel FETs with graphite contacts showed clear ambipolar behavior and switching properties with an on/off ratio of ≈105. A shift in the gate voltage at the minimum conductivity point to a negative value was observed by lowering the vacuum level. In addition, it was found that the SS decreased as the vacuum level was lowered, indicating a reduction in the interfacial trapped charge density due to the physisorption of O_2/H_2O molecules. The electrical properties of the 1L-$MoTe_2$ channel FETs fabricated by gold-mediated exfoliation were strongly affected by the environmental conditions, and these findings are useful for developing FET-type gas sensors.

4. Experimental Section

Schematics of the fabrication process and the 1L-$MoTe_2$ channel device structure are shown in Figure S1 (see Section S1, Supporting Information). 1) First, bulk $MoTe_2$ crystals were mechanically exfoliated using a commonly available Nitto SPV 224R tape. 2) Gold was deposited on the exfoliated $MoTe_2$ crystals by thermal evaporation. 3) The gold film was peeled off together with the top layer of the $MoTe_2$ crystals using thermal release tape (TRT). The exfoliation of the single topmost $MoTe_2$ layer was attributed to the stronger adhesion strength between the topmost layer of $MoTe_2$ and the evaporated gold than the van der Waals forces in the bulk $MoTe_2$ crystal. 4) The exfoliated gold/1L-$MoTe_2$ structures on the TRT were transferred onto a highly doped Si substrate with a 290 nm-thick SiO_2 film. 5) The gold film surface was selectively etched using a mixed aqueous solution consisting of KI (4 g), I_2 (1 g), and H_2O (50 mL). Next, graphite and hBN multilayers were prepared by mechanical tape exfoliation on a polydimethylsiloxane sheet. These flakes were successively picked by a stamping technique using polypropylene carbonate with a lens shape.[43,44] 6) The hBN/graphite structures were stacked directly on the 1L-$MoTe_2$ formed by the Au-mediated exfoliation. The graphite crystals were used as the source and drain electrodes in the device. Finally, the FET structures were annealed at 200 °C for 15 min to remove the residues at the 2D material interfaces.[25]

A standard confocal microscope with a focusing diameter of ≈2 μm was used to observe PL signals from 1L-$MoTe_2$. Spectrally and spatially resolved PL measurements were performed using a continuous-wave laser with an emission wavelength of 532 nm coupled to a 60× microscope objective with a long working distance. PL signals were collected in a backscattering geometry and detected using a liquid-nitrogen-cooled InGaAs detector with a spectrometer. For the PL measurements, the excitation power was maintained at 100 μW to avoid the spectral shape changes due to power-dependent behavior.[45] For electrical measurements, the devices were placed in a cryostat equipped with an electrical feedthrough, with the measurement temperature varied in the range of 180–300 K. A gate voltage V_G was applied to the highly doped Si substrate.

Supporting Information

Supporting Information is available from the Wiley Online Library or from the author.

Acknowledgements

Y.H. acknowledges the support from JSPS KAKENHI (grant nos. JP JP21K04812 and JP24K08206). K.W. and T.T. acknowledge support from JSPS KAKENHI (grant nos. 20H00354 and 23H02052) and the World Premier International Research Center Initiative (WPI), MEXT, Japan.

Conflict of Interest

The authors declare no conflict of interest.

Data Availability Statement

The data that support the findings of this study are available from the corresponding author upon reasonable request.

Keywords

exfoliations, field-effect transistors, molybdenum ditelluride, monolayers

Received: July 24, 2024
Revised: October 13, 2024
Published online: November 21, 2024

[1] H. Zeng, J. Dai, W. Yao, D. Xiao, X. Cui, *Nat. Nanotechnol.* **2012**, *7*, 490.
[2] H. Zhu, Y. Wang, J. Xiao, M. Liu, S. Xiong, Z. J. Wong, Z. Ye, Y. Ye, X. Yin, X. Zhang, *Nat. Nanotechnol.* **2015**, *10*, 151.
[3] A. Castellanos-Gomez, R. van Leeuwen, M. Buscema, H. S. J. van der Zant, G. A. Steele, W. J. Venstra, *Adv. Mater.* **2013**, *25*, 6719.
[4] Y. Tong, Z. Lin, J. T. L. Thong, D. S. H. Chan, C. Zhu, *Appl. Phys. Lett.* **2015**, *107*, 123105.
[5] Y. Kim, S.-K. Kang, N.-C. Oh, H.-D. Lee, S.-M. Lee, J. Park, H. Kim, *ACS Appl. Mater. Interfaces* **2019**, *11*, 38902.
[6] C. Jiang, Q. Li, J. Huang, S. Bi, R. Ji, Q. Guo, *ACS Appl. Mater. Interfaces* **2020**, *12*, 41991.
[7] Z. Feng, Y. Xie, J. Chen, Y. Yu, S. Zheng, R. Zhang, Q. Li, X. Chen, C. Sun, H. Zhang, W. Pang, J. Liu, D. Zhang, *2D Mater.* **2017**, *4*, 025018.
[8] E. Lee, Y. S. Yoon, D.-J. Kim, *ACS Sens.* **2018**, *3*, 2045.
[9] R. Kumar, W. Zheng, X. Lium, J. Zhang, M. Kumar, *Adv. Mater. Technol.* **2020**, *5*, 1901062.
[10] S. Nakaharai, M. Yamamoto, K. Ueno, Y.-F. Lin, S.-L. Li, K. Tsukagoshi, *ACS Nano* **2015**, *9*, 5976.
[11] S. Aftab, S. Samiya, S. Rabia, S. Yousuf, M. U. Khan, R. Khawar, A. Younus, M. Manzoor, M. W. Iqbal, M. Z. Iqbal, *Nanoscale* **2020**, *12*, 15687.
[12] Y.-F. Lin, Y. Xu, S.-T. Wang, S.-L. Li, M. Yamamoto, A. Aparecido-Ferreira, W. Li, H. Sun, S. Nakaharai, W.-B. Jian, K. Ueno, K. Tsukagoshi, *Adv. Mater.* **2014**, *26*, 3263.
[13] S. Nakaharai, M. Yamamoto, K. Ueno, K. Tsukagoshi, *ACS Appl. Mater. Interfaces* **2016**, *8*, 14732.
[14] C. Ruppert, B. Aslan, T. F. Heinz, *Nano Lett.* **2014**, *14*, 6231.
[15] E. Wu, Y. Xie, B. Yuan, H. Zhang, X. Hu, J. Liu, D. Zhang, *ACS Sens.* **2018**, *3*, 1719.
[16] S.-H. Yang, C.-Y. Lin, Y.-M. Chang, M. Li, K.-C. Lee, C.-F. Chen, F.-S. Yang, C.-H. Lien, K. Ueno, K. Watanabe, T. Taniguchi, K. Tsukagoshi, Y.-F. Lin, *ACS Appl. Mater. Interfaces* **2019**, *11*, 47047.
[17] T. A. Empante, Y. Zhou, V. Klee, A. E. Nguyen, I. H. Lu, M. D. Valentin, S. A. N. Alvillar, E. Preciado, A. J. Berges,

C. S. Merida, M. Gomez, S. Bobek, M. Isarraraz, E. J. Reed, L. Bartels, *ACS Nano* **2017**, *11*, 900.
[18] H. Liu, T. Zhang, P. Wu, H. W. Lee, Z. Liu, T. W. Tang, S.-Y. Tang, T. Kang, J.-H. Park, J. Wang, K. Zhang, X. Zheng, Y.-R. Peng, Y.-L. Chueh, Y. Liu, T. Palacios, J. Kong, Z. Luo, *Nano Lett.* **2024**, *24*, 8277.
[19] S. Song, D. H. Keum, S. Cho, D. Perello, Y. Kim, Y. H. Lee, *Nano Lett.* **2016**, *16*, 188.
[20] S. B. Desai, S. R. Madhvapathy, M. Amani, D. Kiriya, M. Hettick, M. Tosun, Y. Zhou, M. Dubey, *Adv. Mater.* **2016**, *28*, 4053.
[21] M. Velický, G. E. Donnelly, W. R. Hendren, S. McFarland, D. Scullion, W. J. I. DeBenedetti, G. C. Correa, Y. Han, A. J. Wain, M. A. Hines, D. A. Muller, K. S. Novoselov, H. D. Abruña, R. M. Bowman, E. J. G. Santos, F. Huang, *ACS Nano* **2018**, *12*, 10463.
[22] F. Liu, W. Wu, Y. Bai, S. H. Chae, Q. Li, J. Wang, J. Hone, X.-Y. Zhu, *Science* **2020**, *367*, 903.
[23] B. Chen, H. Sahin, A. Suslu, L. Ding, M. I. Bertoni, F. M. Peeters, S. Tongay, *ACS Nano* **2015**, *9*, 5326.
[24] S. Larentis, B. Fallahazad, H. C. P. Movva, K. Kim, A. Rai, T. Taniguchi, K. Watanabe, S. K. Banerjee, E. Tutuc, *ACS Nano* **2017**, *11*, 4832.
[25] S. Hayashida, R. Saitoh, K. Watanabe, T. Taniguchi, K. Sawano, Y. Hoshi, *ACS Appl. Electron. Mater.* **2020**, *2*, 2739.
[26] S. Muranaka, S. Nogamida, K. O. Hara, K. Sawano, Y. Hoshi, *AIP Adv.* **2023**, *13*, 075219.
[27] H. Zhu, Q. Wang, L. Cheng, R. Addou, J. Kim, M. J. Kim, R. M. Wallace, *ACS Nano* **2017**, *11*, 11005.
[28] G. Froehlicher, E. Lorchat, S. Berciaud, *Phys. Rev. B* **2016**, *94*, 085429.
[29] G. Froehlicher, E. Lorchat, F. Fernique, C. Joshi, A. Molina-Sánchez, L. Wirtz, S. Berciaud, *Nano Lett.* **2015**, *15*, 6481.
[30] D. H. Keum, S. Cho, J. H. Kim, D.-H. Choe, H.-J. Sung, M. Kan, H. Kang, J.-Y. Hwang, S. W. Kim, H. Yang, K. J. Chang, Y. H. Lee, *Nat. Phys.* **2015**, *11*, 482.
[31] M. Yamamoto, S. T. Wang, M. Ni, Y.-F. Lin, S.-L. Li, S. Aikawa, W.-B. Jian, K. Ueno, K. Wakabayashi, K. Tsukagoshi, *ACS Nano* **2014**, *8*, 3895.
[32] S. Das, H.-Y. Chen, A. V. Penumatcha, J. Appenzeller, *Nano Lett.* **2013**, *13*, 100.
[33] S. Tongay, T. Schumann, A. F. Hebard, *Appl. Phys. Lett.* **2009**, *95*, 222103.
[34] H. Ji, G. Lee, M.-K. Joo, Y. Yun, H. Yi, J.-H. Park, D. Suh, S. C. Lim, *Appl. Phys. Lett.* **2017**, *110*, 183501.
[35] D. Qu, X. Liu, M. Huang, C. Lee, F. Ahmed, H. Kim, R. S. Ruoff, J. Hone, W. J. Yoo, *Adv. Mater.* **2017**, *29*, 1606433.
[36] D.-H. Lien, S. Z. Uddin, M. Yeh, M. Amani, H. Kim, *Science* **2019**, *364*, 468.
[37] R. Peng, Y. Wu, B. Wang, R. Shi, L. Xu, T. Pan, J. Guo, B. Zhao, C. Song, Z. Fan, C. Wang, P. Zhou, S. Fan, K. Liu, *Nat. Electron.* **2023**, *6*, 852.
[38] M. W. Iqbal, H. Ateeq, A. Marriam, M. Manzoor, S. Aftab, S. Azam, E. Elahi, M. M. Faisal, *Microelectron. Eng.* **2022**, *265*, 111885.
[39] Y.-M. Chang, S.-H. Yang, C.-Y. Lin, C.-H. Chen, C.-H. Lien, W.-B. Jian, K. Ueno, Y.-W. Suen, K. Tsukagoshi, Y.-F. Lin, *Adv. Mater.* **2018**, *30*, 1706995.
[40] K. Park, H. Kang, S. Koo, D. Lee, S. Ryu, *Nat. Commun.* **2019**, *10*, 4931.
[41] D. Lee, G. Ahn, S. Ryu, *J. Am. Chem. Soc.* **2014**, *136*, 6634.
[42] J. C. Kotsakidis, Q. Zhang, A. L. Vazquez de Parga, M. Currie, K. Helmerson, D. K. Gaskill, M. S. Fuhrer, *Nano Lett.* **2019**, *19*, 5205.
[43] Y. Hoshi, M. Okada, R. Moriya, S. Masubuchi, K. Watanabe, T. Taniguchi, R. Kitaura, T. Machida, *Phys. Rev. Mater.* **2018**, *2*, 064003.
[44] S. Toyoda, T. Uwanno, T. Taniguchi, K. Watanabe, K. Nagashio, *Appl. Phys. Express* **2019**, *12*, 055008.
[45] Y. Hoshi, T. Kuroda, M. Okada, R. Moriya, S. Masubuchi, K. Watanabe, T. Taniguchi, R. Kitaura, T. Machida, *Phys. Rev. B* **2017**, *95*, 241403.